



CHEMISTRY & SUSTAINABILITY

# CHEM **SUS** CHEM

ENERGY & MATERIALS

## Accepted Article

**Title:** Adjusting the introduction of cations (MA, Cs or Rb) to obtain highly efficient and stable perovskite solar cells based on (FAPbI<sub>3</sub>)<sub>0.9</sub>(FAPbBr<sub>3</sub>)<sub>0.1</sub>

**Authors:** Guozhen Liu, Haiying Zheng, Liangzheng Zhu, Ahmed Alsaedi, Tasawar Hayat, Xu Pan, Li'e Mo, and Songyuan Dai

This manuscript has been accepted after peer review and appears as an Accepted Article online prior to editing, proofing, and formal publication of the final Version of Record (VoR). This work is currently citable by using the Digital Object Identifier (DOI) given below. The VoR will be published online in Early View as soon as possible and may be different to this Accepted Article as a result of editing. Readers should obtain the VoR from the journal website shown below when it is published to ensure accuracy of information. The authors are responsible for the content of this Accepted Article.

**To be cited as:** *ChemSusChem* 10.1002/cssc.201800658

**Link to VoR:** <http://dx.doi.org/10.1002/cssc.201800658>

WILEY-VCH

[www.chemsuschem.org](http://www.chemsuschem.org)

A Journal of



# Adjusting the introduction of cations (MA, Cs or Rb) to obtain highly efficient and stable perovskite solar cells based on (FAPbI<sub>3</sub>)<sub>0.9</sub>(FAPbBr<sub>3</sub>)<sub>0.1</sub>

Guozhen Liu,<sup>[a,b]</sup> Haiying Zheng,<sup>[a,b]</sup> Liangzheng Zhu,<sup>[a,b]</sup> Ahmed Alsaedi<sup>[c]</sup>, Tasawar Hayat<sup>[c,e]</sup>, Xu Pan,<sup>\*[a]</sup> Li'e Mo<sup>\*[a]</sup> and Songyuan Dai<sup>\*[a,c,d]</sup>

<sup>a</sup>Key Laboratory of Photovoltaic and Energy Conservation Materials, Institute of Applied Technology, Hefei Institutes of Physical Science, Chinese Academy of Sciences, Hefei 230031, China.

<sup>b</sup>University of Science and Technology of China, Hefei 230026, China.

<sup>c</sup>NAAM Research Group, Department of Mathematics, Faculty of Science, King Abdulaziz University, Jeddah 21589, Saudi Arabia.

<sup>d</sup>State Key Laboratory of Alternate Electrical Power System with Renewable Energy Sources, North China Electric Power University, Beijing 102206, China.

<sup>e</sup>Department of Mathematics, Quaid-I-Azam University, Islamabad 44000, Pakistan.

E-mail: xpan@rntek.cas.cn, lemo@rntek.cas.cn, sydai@ncepu.edu.cn

**Abstract:** Although power conversion efficiency (PCE) of perovskite solar cells (PSCs) has increased to 22.7%, the instability when exposed to moisture and heat hindered their further practical development. In this study, to gain highly efficient and stable perovskite component, MA, Cs and Rb cations are respectively introduced into the (FAPbI<sub>3</sub>)<sub>0.9</sub>(FAPbBr<sub>3</sub>)<sub>0.1</sub> film which is rarely used due to the poor photovoltaic performance. The effects of different contents of MA, Cs or Rb cations on the performance of (FAPbI<sub>3</sub>)<sub>0.9</sub>(FAPbBr<sub>3</sub>)<sub>0.1</sub> films and devices are systematically studied.

The results show that the devices with Cs cation exhibit markedly improved photovoltaic performance and stability, attributing to the obviously enhanced quality of films and their intrinsic stability. The  $(\text{FAPbI}_3)_{0.9}(\text{FAPbBr}_3)_{0.1}$  devices with 10% Cs obtain a PCE as high as 19.94%. More importantly, the unsealed devices retain about 80% and 90% of the initial PCE at 85 °C after 260 h and under 45±5% relative humidity (RH) after 1440 h, respectively, which are more brilliant than that with 15% MA and 5% Rb under the same condition. It indicates that a highly efficient and stable perovskite component has been achieved and the PSCs based on this component will expect to promote the further development.

**Keywords:** perovskite solar cells, cations introduction, high efficiency, humidity stability, thermal stability

## Introduction

In the last few years, organic-inorganic metal halide perovskite solar cells (PSCs) have attracted unprecedented attention and been supposed to be one of the most promising superstar for next-generation photovoltaic industry due to their outstanding properties, such as wide absorption band, low defect density, high charge carrier mobility and long diffusion length.<sup>[1-9]</sup> Recently, the certified power conversion efficiency (PCE) in laboratory has increased to 22.7%,<sup>[10]</sup> which has surpassed the records of the second-generation solar cell kept by CIGS/CdTe and been still continuously updated.<sup>[11]</sup>

Unfortunately, the poor stability of PSCs under high humidity and temperature have been reported to impede their commercialized development.<sup>[12-15]</sup> More and more attempts have been proposed to enhance the humidity and temperature stability of PSCs, such as changing the electron transport materials (ETM),<sup>[16,17]</sup> introducing the additives into light absorber layer,<sup>[18-21]</sup> employing the inorganic hole-transporting materials (HTM) without dopant.<sup>[22,23]</sup>

Among these efforts, to obtain a stability perovskite material by compositional engineering is one of the simplest and most essential method.<sup>[24-29]</sup> Pure FAPbI<sub>3</sub> suffers from poor humidity stability due to the easy phase transition from the  $\alpha$ -phase perovskite (black) to the  $\delta$ -phase nonperovskite (yellow), which hinders its intensive study and widespread use.<sup>[24,27]</sup> Seok and co-workers<sup>[30]</sup> introduced MAPbBr<sub>3</sub> component into FAPbI<sub>3</sub> to gain (FAPbI<sub>3</sub>)<sub>0.85</sub>(FAPbBr<sub>3</sub>)<sub>0.15</sub> PSCs which present high PCE and phase stability. Park and co-workers<sup>[31]</sup> adopted inorganic Rb<sup>+</sup> as an enhancer to improve the photovoltaic performance and moisture stability of FAPbI<sub>3</sub> PSCs. Zhou and co-workers<sup>[32]</sup> acquired highly efficient and stable FA<sub>1-x</sub>Cs<sub>x</sub>PbI<sub>3</sub>(Cl) PSCs by the intercalation of CsI. Moreover, (FAPbI<sub>3</sub>)<sub>1-y</sub>(FAPbBr<sub>3</sub>)<sub>y</sub> have been supposed to be more stable, whereas they are rarely used in solar cells due to the poor photovoltaic performance.<sup>[33,34]</sup> Therefore, it is an urgent need to improve the PCE and stability of devices based on this component.

In this study, we report embedding different contents of MA, Cs or Rb cations into (FAPbI<sub>3</sub>)<sub>0.9</sub>(FAPbBr<sub>3</sub>)<sub>0.1</sub> perovskite film to fabricate highly efficient and stable PSCs. Finally, a perovskite composition exhibits superior photovoltaic performance and

excellent stability by introducing 10% Cs into  $(\text{FAPbI}_3)_{0.9}(\text{FAPbBr}_3)_{0.1}$  film. The devices with a PCE of 19.94% under AM 1.5G solar illumination can be achieved due to the excellent photoelectric property and film quality. In addition, the unsealed devices display remarkable humidity and heat stability after aging at 85 °C and under  $45\pm 5\%$  relative humidity (RH), respectively, which is more outstanding than the composition by introducing 15% MA and 5% Rb.

## Results and discussion

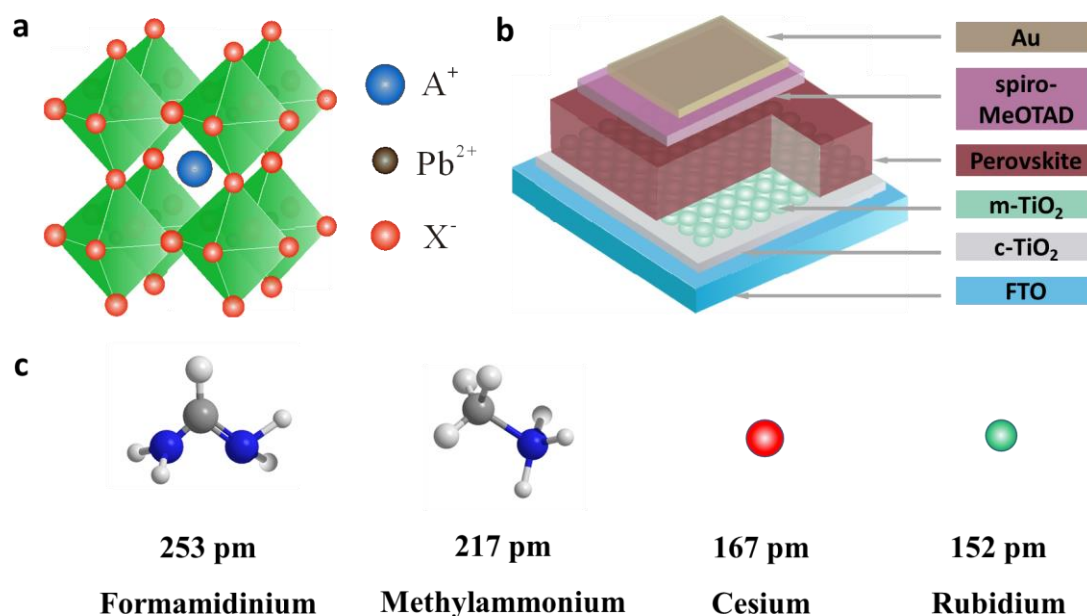


**Figure 1.** (a) Crystal structure of  $\text{APbX}_3$  perovskite. (b) Schematic architecture of mesoscopic PSC. (c) Ionic structures and radius of different A-site cations (FA, MA, Cs and Rb).

Herein, based on the  $(\text{FAPbI}_3)_{0.9}(\text{FAPbBr}_3)_{0.1}$  component, different perovskite films were fabricated by one-step method. The schematic architecture of mesoscopic PSC is depicted in Figure 1b. The ionic structure and radius of four different A-site cations

(FA, MA, Cs and Rb) are shown in Figure 1c. After introducing different contents of cations (MA, Cs or Rb), we prepared  $(A_xFA_{1-x}PbI_3)_{0.9}(FAPbBr_3)_{0.1}$  films with  $x$  ranging from 0 to 0.05, 0.1 and 0.15 (Labeled as FA, A<sub>5</sub>-FA, A<sub>10</sub>-FA and A<sub>15</sub>-FA for easy recognition, A= MA, Cs or Rb), respectively.

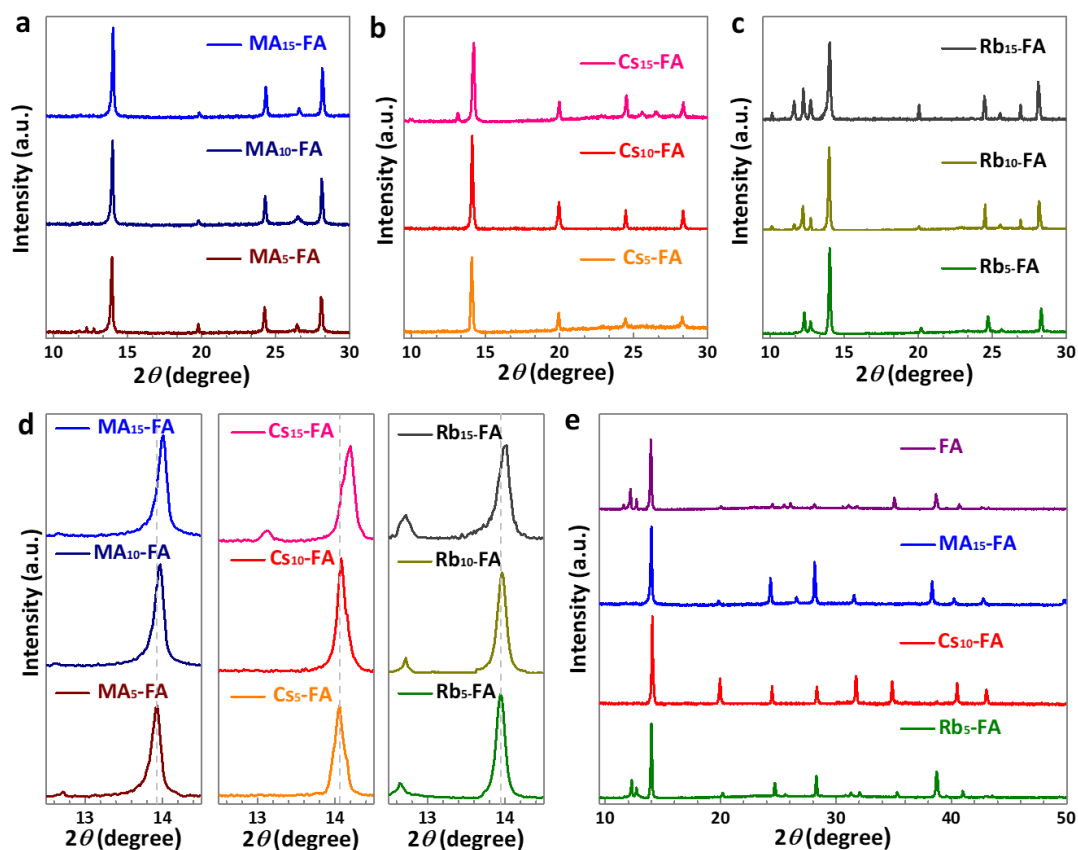


**Figure 2.** XRD patterns of (a) MA<sub>x</sub>-FA, (b) Cs<sub>x</sub>-FA and (c) Rb<sub>x</sub>-FA ( $x=5, 10$  and  $15$ ) perovskite films. (d) The magnified XRD patterns of the (110) peak of MA<sub>x</sub>-FA, Cs<sub>x</sub>-FA and Rb<sub>x</sub>-FA ( $x=5, 10$  and  $15$ ) perovskite films. (e) XRD patterns of FA, MA<sub>15</sub>-FA, Cs<sub>10</sub>-FA and Rb<sub>5</sub>-FA perovskite films.

To uncover the crystal structure of perovskite films after introducing different cations (MA, Cs or Rb), XRD patterns are shown in Figure 2. Figure 2a, b and c demonstrate the XRD patterns of perovskite films with different contents of MA, Cs

and Rb, respectively. After introducing MA or Cs cations, the films display good crystallinity of  $\alpha$ -phase perovskites. As shown in Figure 2a, when the content of MA cation is 5%, the diffraction peaks at  $12.2^\circ$  and  $12.7^\circ$  are attributed to the “orange-red” phase and residual  $\text{PbI}_2$  presenting in the films.<sup>[35]</sup> In Figure 2b, when the content of Cs cation increases to 15%, there is a weak diffraction peak at  $13.12^\circ$ , which can be speculated as the formation of  $\delta\text{-CsPbI}_3$ .<sup>[31]</sup> However, the  $\text{Rb}_x\text{-FA}$  films in Figure 2c have poor crystalline structure. As the content of Rb only increases beyond 5%, the diffraction peaks at  $10.1^\circ$  and  $26.9^\circ$  indicate the formation of  $\delta\text{-RbPbI}_3$ . It is attributable to the big difference in ionic radius between Rb (152 pm) and FA (253 pm).<sup>[31]</sup> In Figure 2d, with the increase of MA cation content from 5% to 10% and 15%, the diffraction peaks attributed to (110) plane of  $\alpha\text{-FAPbI}_3$  display a little shift to higher angle, in agreement with the smaller size of MA cation relative to FA, which shrinks the crystal lattice.<sup>[34]</sup> The same shifts can be found in  $\text{Cs}_x\text{-FA}$  and  $\text{Rb}_x\text{-FA}$  perovskite films. On the one hand, it may be caused by the lattice distortion after inserting of a cation (Cs or Rb) smaller than FA cation.<sup>[31,40]</sup> On the other hand, the Cs and Rb cations may be acted as scavengers to eliminate iodide selectively (resulting in the blue shift in UV-vis absorption spectra and PL spectra) or by regulate the vacancies through the incorporation of excess cations/anions from the addition of excess AX (CsI or RbI). The real reason is very valuable to explore in the further work. As a result, Cs and Rb cations play a role in preventing bromide phase-segregation of the perovskite effectively.

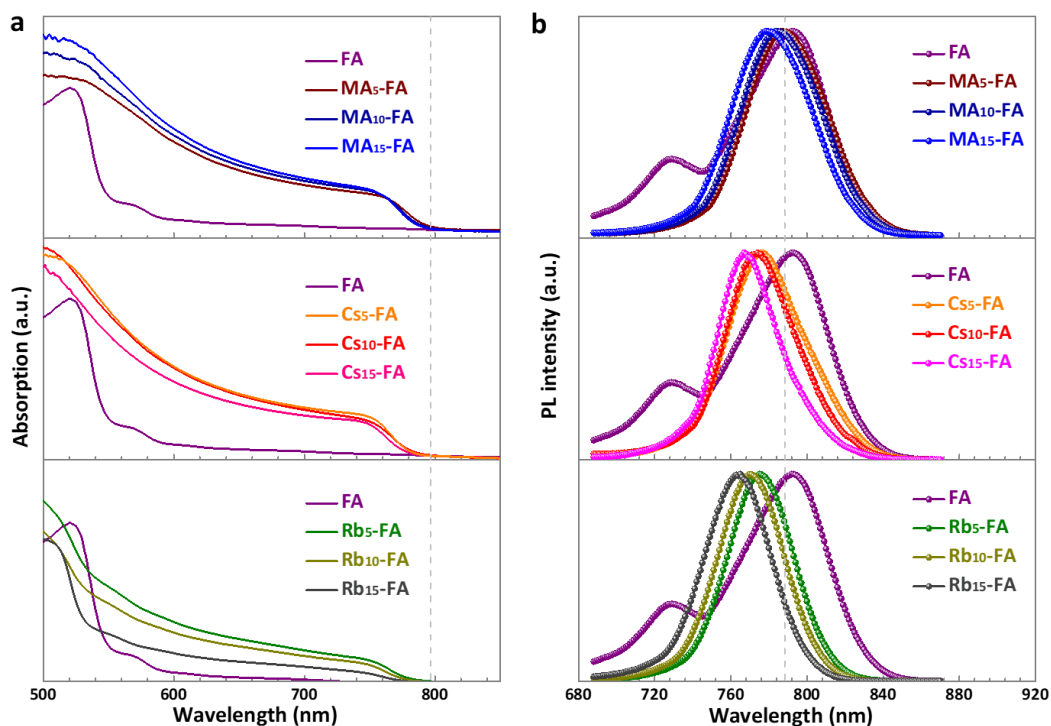


**Figure 3.** (a) UV-vis absorption spectra and (b) normalized PL spectra of FA, MA<sub>x</sub>-FA, Cs<sub>x</sub>-FA and Rb<sub>x</sub>-FA (x=5, 10, and 15) perovskite films.

To make clear the different influence of mixed cations (MA, Cs or Rb) on the crystallization, Figure 2e shows the XRD patterns of (FAPbI<sub>3</sub>)<sub>0.9</sub>(FAPbBr<sub>3</sub>)<sub>0.1</sub> film and perovskite films with MA, Cs or Rb cations in the case of the optimal proportion. Without any mixed cations, the film owns an obvious diffraction peak at about 12.23°, suggesting the formation of a new material or phase which displays as orange-red.<sup>[32]</sup> The diffraction peaks at about 11.6° and 12.7° are attributed to the  $\delta$ -phase of FAPbI<sub>3</sub> and residual PbI<sub>2</sub>, respectively, which are common phenomena in FA-based PSCs and lead to reduced properties.<sup>[25,31]</sup> Whereas, for the MA<sub>15</sub>-FA and Cs<sub>10</sub>-FA films, no diffraction peaks are observed around 11.61°, 12.23° and 12.69°, indicating that there are no  $\delta$ -phase of FAPbI<sub>3</sub>, “orange-red” phase and residual PbI<sub>2</sub> in the films. With regards to Rb<sub>5</sub>-FA film, obvious diffraction peaks can be found at about 12.2° and 12.7°.

It means that, compared with MA and Cs, the introducing of Rb cation takes the weakest majorization of promoting great crystallinity of  $\alpha$ -phase perovskites. The results are consistent with the performance of the corresponding devices.

The UV-vis absorption spectra and normalized PL spectra are utilized to examine the optical properties of  $(\text{FAPbI}_3)_{0.9}(\text{FAPbBr}_3)_{0.1}$  perovskite films with different contents of mixed cations (MA, Cs or Rb). As shown in Figure 3a, after introducing MA, Cs or Rb cations, all the films exhibit visibly enhanced light absorption from 550 to 800 nm due to the improved crystallinity. For  $\text{Rb}_x\text{-FA}$ , the poor light absorption may owe to the easily separated of  $\delta\text{-RbPbI}_3$  from the films. A slight blue-shift can be observed as the increase of cations (MA, Cs or Rb) contents, which is in good agreement with the corresponding PL peaks in Figure 3b. Compared to  $\text{MA}_x\text{-FA}$ , the  $\text{Cs}_x\text{-FA}$  and  $\text{Rb}_x\text{-FA}$  films present a blue shift in absorption band edge because of the smaller ionic radius of Cs and Rb. The same trend can be found on the normalized PL spectra. Interestingly, a second peak can be found in the PL spectra of FA film (Figure 3b), which is caused by the phase-segregated consisting of Br-rich and Br-free regions.<sup>[38,39]</sup> The second phase (orange-red phase) displays a XRD diffraction peak at  $2\theta = 12.23^\circ$  (Figure 2e). It is a simply intrinsic to all  $(\text{FAPbI}_3)_{1-x}(\text{FAPbBr}_3)_x$  perovskite compositions (Figure S7) and the potential reason for  $(\text{FAPbI}_3)_{1-x}(\text{FAPbBr}_3)_x$  devices behave a poorer photovoltaic property. When introducing mixed cations (MA, Cs or Rb), no second PL peak is observed. The results demonstrate that the existence of mixed cations (MA, Cs or Rb) in the  $(\text{FAPbI}_3)_{0.9}(\text{FAPbBr}_3)_{0.1}$  films can effectively restrain the phase separation. This conclusion is consistent with the result of the XRD patterns.

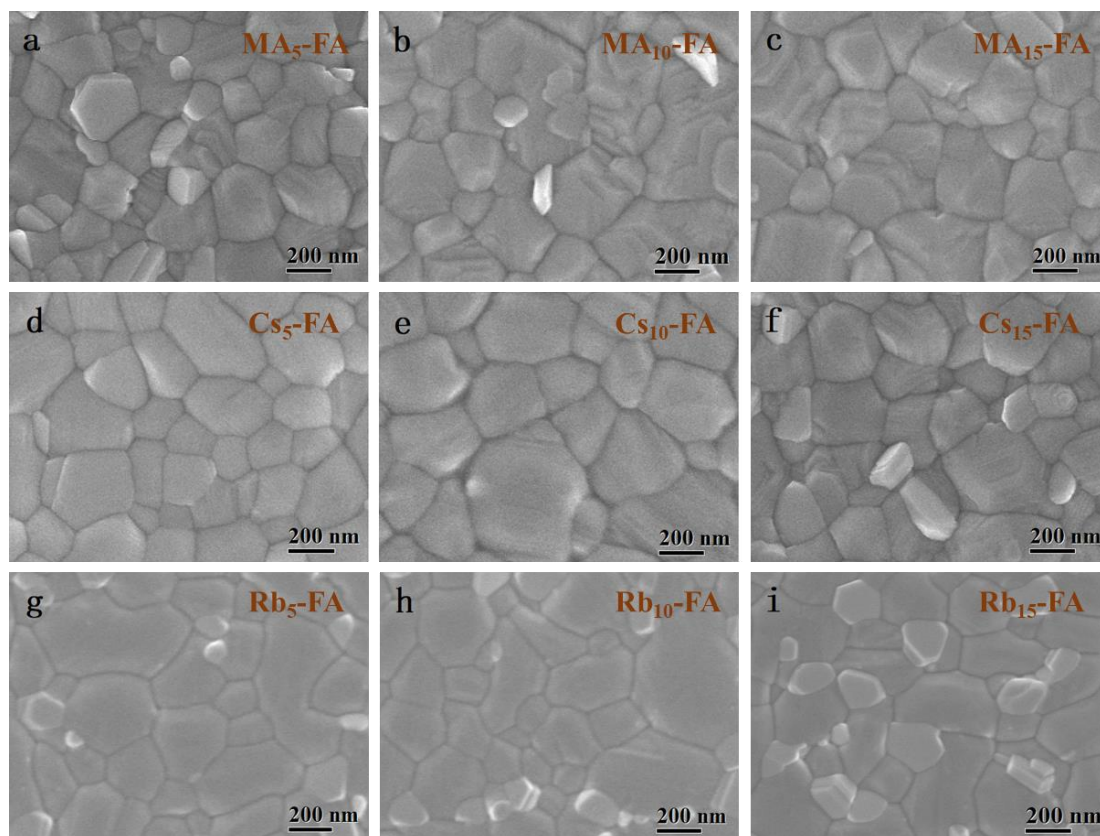


**Figure 4.** Top surface SEM images of MA<sub>x</sub>-FA, Cs<sub>x</sub>-FA and Rb<sub>x</sub>-FA (x=5, 10 and 15) perovskite films.

Scanning electron microscopy (SEM) measurements are used to perform the surface morphology of (FAPbI<sub>3</sub>)<sub>0.9</sub>(FAPbBr<sub>3</sub>)<sub>0.1</sub> perovskite films with mixed cations (MA, Cs or Rb). Figure 4 shows the top surface SEM images of mixed cations perovskite films with different contents. In the experiment, all the films display compact surface without pinhole. Among the films with increased contents of MA cation, the morphologies turn to be smooth. In addition, when the contents of Cs and Rb cations increases to 15%, the morphologies (Cs<sub>15</sub>-FA and Rb<sub>15</sub>-FA) are rough and there are many irregular crystals growing on the surfaces. Those could be caused by the formation of  $\delta$ -CsPbI<sub>3</sub> and  $\delta$ -RbPbI<sub>3</sub>, respectively. Especially, the films with 15% MA

and 10% Cs present relatively smooth and uniform top surface, which will effectively reduce the defect and then improve the photoelectricity properties.

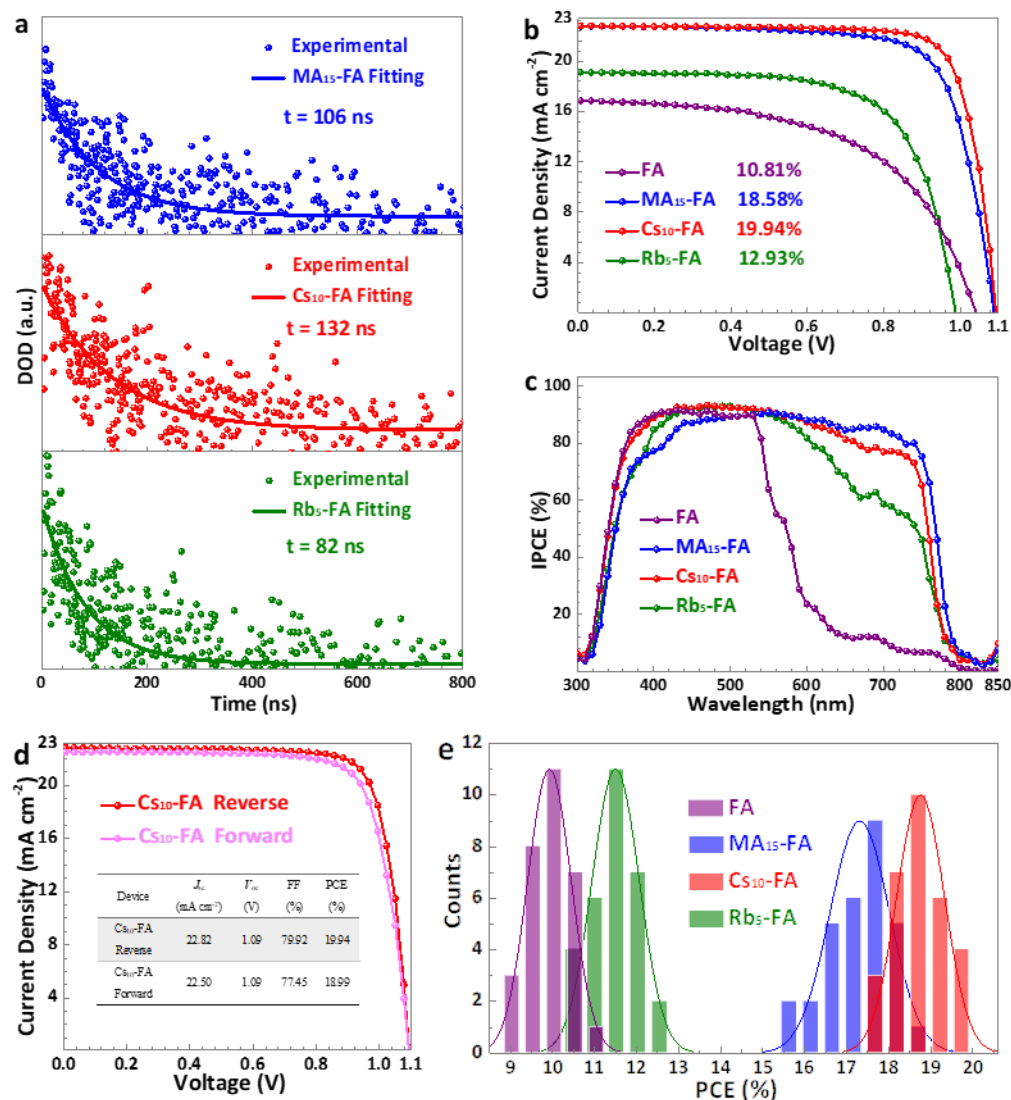


**Figure 5.** (a) Normalized transient absorption (TA) responses of glass/perovskite films (MA<sub>15</sub>-FA, Cs<sub>10</sub>-FA and Rb<sub>5</sub>-FA). (b)  $J-V$  curves and (c) incident photon to current conversion efficiency (IPCE) spectra of PSCs based on FA, MA<sub>15</sub>-FA, Cs<sub>10</sub>-FA and Rb<sub>5</sub>-FA perovskite films. (d)  $J-V$  curves of Cs<sub>10</sub>-FA PSC under reverse and forward scan directions. (e) The PCE histogram fitted with a Gaussian distribution of the FA, MA<sub>15</sub>-FA, Cs<sub>10</sub>-FA and Rb<sub>5</sub>-FA devices among 30 measured devices.

To investigate the recombination behavior between electron and hole in the perovskite layer with different components, we measured transient absorption (TA) spectra (Figure 5a). The internal recombination occurred in perovskite layers has a great influence on the photovoltaic performance of devices. The longer recombination time means the slower recombination of electron and hole, leading to better device performance.<sup>[36,37]</sup> According to fitting results in single exponential decays, the Cs<sub>10</sub>-FA has the longest lifetime of 132 ns, which is 106 ns and 82 ns for MA<sub>15</sub>-FA and Rb<sub>5</sub>-FA, respectively. The Rb<sub>5</sub>-FA displays the shortest lifetime due to its worse crystallization and morphology. In other words, a high-quality film with perfect morphology and fewer defect states could be achieved by introducing 10% Cs cation.

To further characterize the photovoltaic performance of perovskite films, the devices with structure of FTO/c-TiO<sub>2</sub>/m-TiO<sub>2</sub>/perovskite/spiro-MeOTAD/Au were fabricated by introducing different contents of mixed cations (MA, Cs or Rb) into (FAPbI<sub>3</sub>)<sub>0.9</sub>(FAPbBr<sub>3</sub>)<sub>0.1</sub> perovskite photoactive layer. The current–voltage (*J–V*) curves and corresponding parameters measured under standard AM1.5G illumination are shown in Figure 5b and Table 1, respectively. The device based on (FAPbI<sub>3</sub>)<sub>0.9</sub>(FAPbBr<sub>3</sub>)<sub>0.1</sub> film displays an inferior PCE of 10.81% with a much lower *J*<sub>sc</sub> of 14.95 mA cm<sup>-2</sup>, which is caused by the presence of orange-red phase. Fortunately, by introducing mixed cations into the perovskite films, the photoelectric property can be increased effectively, due to the adjustment of bandgap and the improvement of absorption. Among the PSCs with different components, the MA<sub>15</sub>-FA and Cs<sub>10</sub>-FA devices own a better performance, which is in accord with the crystallization,

morphology and TA characterization. Particularly, the device based on the Cs<sub>10</sub>-FA gains the optimal photovoltaic performance with a  $J_{sc}$  of 22.82 mA cm<sup>-2</sup>, a  $V_{oc}$  of 1.09 V, and a FF of 79.92%, and ultimately an excellent PCE of 19.94%. When refer to Rb<sub>5</sub>-FA, the  $V_{oc}$  is as low as 0.99 V, which can be put down to the worse film quality. The incident photon to current conversion efficiency (IPCE) spectra of the optimal devices are shown in Figure 5c. The results are consistent with the  $J_{sc}$  presenting in corresponding  $J$ - $V$  curves. A slight blue shift also can be find which has mentioned in the UV-vis absorption spectra (Figure 3a). The hysteresis phenomenon, an important index to evaluate the actual photovoltaic performances, is verified by collecting  $J$ - $V$  curves under reverse and forward scan directions. In Figure 5d, the results exhibit that the device with a component of Cs<sub>10</sub>-FA has a 0.95% PCE hysteresis, which is lower than most reported FA-based PSCs.<sup>[25,32]</sup> Moreover, Figure 5e presents PCE histograms of different devices with a Gaussian distribution. An apparent variation of PCE can be observed among the four kinds of PSCs. When refer to Cs<sub>10</sub>-FA, an average PCE of 18.81% can be achieved among 30 measured devices, indicating a high reproducibility.

**Table 1.** Photovoltaic parameters of FA, MA<sub>15</sub>-FA, Cs<sub>10</sub>-FA and Rb<sub>5</sub>-FA PSCs.

Device	$J_{sc}$ (mA cm <sup>-2</sup> )	$V_{oc}$ (V)	FF (%)	PCE (%)
FA	16.86	1.04	61.55	10.81
MA <sub>15</sub> -FA	22.77	1.09	74.89	18.58
Cs <sub>10</sub> -FA	22.82	1.09	79.92	19.94
Rb <sub>5</sub> -FA	19.12	0.99	68.33	12.93

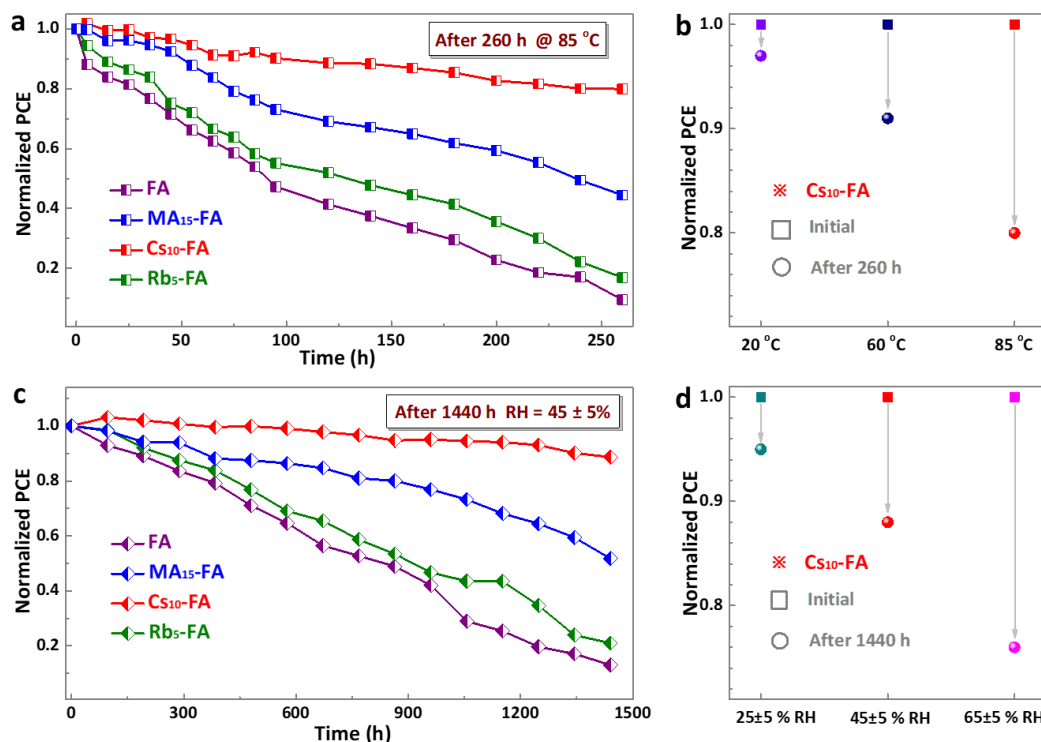


**Figure 6.** Normalized PCE variation curves of unsealed FA, MA<sub>15</sub>-FA, Cs<sub>10</sub>-FA and Rb<sub>5</sub>-FA PSCs when exposure to (a) 85 °C and (c) 45 ± 5% RH. (b) Thermal stability measurements for Cs<sub>10</sub>-FA PSCs at different temperatures: 20, 60 and 85 °C. (d) Humidity stability measurements for Cs<sub>10</sub>-FA PSCs under different humidity: 25 ± 5%, 45 ± 5%, and 65 ± 5% RH.

The instability of PSCs which are prone to degradation upon exposure to moisture and heat has hindered their realistic development. Therefore, it is a serious matter to improve the stability of PSCs. We firstly measured the thermal stability of high performance four kinds of devices (FA, MA<sub>15</sub>-FA, Cs<sub>10</sub>-FA and Rb<sub>5</sub>-FA) stored in the condition of 85 °C where the RH is about 20% without any encapsulation (in the dark). Figure 6a shows the normalized PCE variation curves as a function of the testing time. Compared with Rb<sub>5</sub>-FA and FA devices, which only retain about 18% and 10% of the initial PCE, respectively, the Cs<sub>10</sub>-FA PSCs display the most outstanding thermal

stability. After aging for 260 hours (h), the best device of Cs<sub>10</sub>-FA only decreases by 20%. Although the MA<sub>15</sub>-FA PSCs display a good stability at the first 50 h, only 45% of the initial values is kept after 260 h. According to GTF calculation, it is easy for MA<sup>+</sup> to desorb from the crystal, which will lead to the thermal instability.<sup>[26]</sup> Meanwhile, the stability of Cs<sub>10</sub>-FA PSCs under 20 °C and 60 °C was also measured (Figure 6b). After 260 h, the PCE only decrease by about 3% and 9%, respectively. In our case, the enhanced thermal stability should be ascribed to the more stable structural of Cs/FA double cations component.

We further conducted the humidity stability of the FA, MA<sub>15</sub>-FA, Cs<sub>10</sub>-FA and Rb<sub>5</sub>-FA devices. Here, the test was proceeding under 45±5% RH at room temperature (in the dark) and all the devices were not encapsulated. It can be found from Figure 6c, after 1440-h aging test, the Cs<sub>10</sub>-FA devices retain about 88% of the initial PCE. Whereas, at the same condition, the PCE of FA, MA<sub>15</sub>-FA and Rb<sub>5</sub>-FA devices decrease by about 87%, 79% and 49%, respectively, while only 12% for the Cs<sub>10</sub>-FA. Furthermore, the Cs<sub>10</sub>-FA PSCs still maintain about 95% and 76% of the initial PCE after aging under 25±5% and 65±5% RH for 1440 h, respectively (Figure 6d). The results exhibit that a device with superior humidity stability can be realized by introducing Cs cation into the (FAPbI<sub>3</sub>)<sub>0.9</sub>(FAPbBr<sub>3</sub>)<sub>0.1</sub> perovskite films.

## Conclusions

In conclusion, we systematically studied the impact of MA, Cs or Rb cations introduction on the performance of (FAPbI<sub>3</sub>)<sub>0.9</sub>(FAPbBr<sub>3</sub>)<sub>0.1</sub> film and device. By

regulating the contents of MA, Cs or Rb cations, perovskite films with different components were fabricated. As a result, the  $(\text{FAPbI}_3)_{0.9}(\text{FAPbBr}_3)_{0.1}$  devices with 10% Cs obtain a highest PCE up to 19.94%, compared to the devices without doping (PCE= 10.81%), with 15% MA (PCE= 18.58%) and 5% Rb (PCE= 12.93%). Meanwhile, the PSCs with 10% Cs display more outstanding stability against moisture and heat than other devices under the same fabricating and aging conditions. The unsealed  $(\text{Cs}_{0.1}\text{FA}_{0.9}\text{PbI}_3)_{0.9}(\text{FAPbBr}_3)_{0.1}$  devices maintain about 80% of their initial PCE under 85 °C after 260 h and the PCE only decrease by about 10% after 1440 h under 45±5% RH. This work provides a valuable method to higher efficient and stable PSCs as a next-generation photovoltaic industry.

## Experimental Section

### Materials and preparation

Formamidinium iodide  $\text{HC}(\text{NH}_2)_2\text{I}$  (FAI) and formamidinium bromide  $\text{HC}(\text{NH}_2)_2\text{Br}$  (FABr): FAI and FABr were prepared by reacting formamidinium acetate powder with 57 wt% hydroiodic acid (for FAI) or 47 wt% hydrobromic acid (for FABr) with stoichiometrically. After adding HI or HBr, the solution was stirred for 2 h in the ice bath. Then, the solution was evaporated at about 55 °C using rotary evaporation to remove the solvent under reduced pressure. The powders were then purified by dissolving in ethanol and recrystallizing in anhydrous ether. Finally, the products were dried in vacuum at 60 °C overnight.

Preparation of perovskite precursors: The  $(\text{FAPbI}_3)_{0.9}(\text{FAPbBr}_3)_{0.1}$  precursor solution ( $1.35 \text{ M Pb}^{2+}$ ) was prepared from dissolving the lead iodide ( $\text{PbI}_2$ ), lead bromine ( $\text{PbBr}_2$ ), formamidinium iodide (FAI) and formamidinium bromine (FABr) powders in mixed solvent of DMSO (20% by volume) and DMF (80% by volume). MAI/CsI/RbI were incorporated into the precursor solution by replacing the corresponding content of FAI. All the solutions were then stirred for 1 h at  $70 \text{ }^\circ\text{C}$  and filtered using  $0.45 \text{ }\mu\text{m}$  PVDF filters before spin-coating.

### Device fabrication

The FTO substrate was washed by sonication for 30 min and sequentially cleaned by ultrapure water and ethanol for several times. The compact layer of  $\text{TiO}_2$  was coated on the substrate by spray pyrolysis at  $450 \text{ }^\circ\text{C}$  with the precursor solution of 7-mL isopropanol, 0.6-mL titanium diisopropoxide and 0.4-mL bis(acetylacetonate). The  $\text{TiO}_2$  mesoporous layer was then spin-coated on the compact layer at 4000 r.p.m for 20 s, followed by 10 min thermal drying at  $100 \text{ }^\circ\text{C}$ . Then, the substrate was annealed at  $510 \text{ }^\circ\text{C}$  for 30 min. After cooling to room temperature, perovskite precursor solution was poured onto the substrate and spin-coated for 50 s (1100 r.p.m for 15 s and then 4600 r.p.m for 35 s) in an air flowing glovebox (About 20%RH). 120- $\mu\text{L}$  chlorobenzene was drop-casted on the rotating film 15 s before the end of the spin coating program. The deposited film was then heated at  $150 \text{ }^\circ\text{C}$  for 30 min when the component is  $(\text{FAPbI}_3)_{0.9}(\text{FAPbBr}_3)_{0.1}$ . When MAI/CsI/RbI were incorporated into the precursor solutions, the deposited film was heated at  $100 \text{ }^\circ\text{C}$  for 30 min. The HTL, with a composed of spiro-OMeTAD (73 mg), 4-tert-butylpyridine (29  $\mu\text{L}$ ), lithium

bis(trifluoromethylsulphonyl) imide (LiTFSI, 17  $\mu\text{L}$ ) and Co(III)-complex (8  $\mu\text{L}$ ) in 1-mL chlorobenzene solvent, was spin-coated on the perovskite film with a speed of 3000 r.p.m for 20 s. Finally, about 60-nm Au electrode were deposited on the HTL by thermal evaporating.

### Characterization

X-ray diffraction (XRD) patterns of perovskite films were recorded on an X'pert PRO MPD (PANalytical) with Cu  $K\alpha$  radiation and the  $2\theta$  range was 10-50°. Ultraviolet-visible (UV-vis) absorption spectra were carried out by an UV-vis spectrophotometer (UV-vis, U-3900H, HITACHI, Japan) with the wavelength range from 500 nm to 900 nm. Steady-state fluorescence (PL) spectra were measured and recorded by a spectrofluorometer (photon technology international), analyzed by a software Fluorescence. The excitation light wavelength was 473 nm from a standard 450 W xenon CW lamp. Scanning electron microscopy (SEM) measurements were performed on a Schottky Field Emission SEM (FEI Sirion200). Transient absorption spectra (TAS) were tested by LKS.80 and LP.920. Incident monochromatic photon-to-current efficiency (IPCE) of perovskite solar cells were recorded by QE/IPCE measurement system (Newport, USA). Photocurrent and voltage curves ( $J-V$ ) were obtained by a solar simulator (Newport, Oriel Class A, 91195A) at 100  $\text{mW}/\text{cm}^2$  illumination AM 1.5G. The active area of devices was defined as 0.09  $\text{cm}^2$  by a black mask. The setup was calibrated with a certified silicon solar cell (Fraunhofer ISE) prior to measurements. The humidity aging tests were measured in the containers remained at room temperature, under dark and the humidity of about 25%, 45% and 65% was controlled

by humidifier and desiccant. The temperature aging tests were measured in the drying ovens with the humidity of about 20% under dark, the temperatures were retained at 20 °C, 60 °C and 85 °C.

## Acknowledgements

This work was financially supported by the National High Technology Research and Development Program of China under Grant No.2015AA050602, STS project of Chinese Academy of Sciences (KFJ-SW-STS-152).

## References

- [1] A. Kojima, K. Teshima, Y. Shirai, T. Miyasaka, *J. Am. Chem. Soc.* **2009**, *131*, 6050-6051.
- [2] J. M. Ball, M. M. Lee, A. Hey, H. J. Snaith, *Energy Environ. Sci.* **2013**, *6*, 1739-1743.
- [3] H. S. Jung, N.-G. Park, *Small* **2015**, *11*, 10-25.
- [4] M. Saliba, T. Matsui, K. Domanski, J.-Y. Seo, A. Ummadisingu, S. M. Zakeeruddin, J.-P. Correa-Baena, W. R. Tress, A. Abate, A. Hagfeldt, M. Grätzel, *Science* **2016**, *354*, 206-209.
- [5] W. S. Yang, B.-W. Park, E. H. Jung, N. J. Jeon, Y. C. Kim, D. U. Lee, S. S. Shin, J. Seo, E. K. Kim, J. H. Noh, S. I. Seok, *Science* **2017**, *356*, 1376-1379.
- [6] M. Grätzel, *Nat. Mater.* **2014**, *13*, 838-842.
- [7] Q. Chen, H. Zhou, Z. Hong, S. Luo, H.-S. Duan, H.-H. Wang, Y. Liu, G. Li, Y. Yang, *J. Am. Chem. Soc.* **2014**, *136*, 622-625.

- [8] Q. Dong, Y. Fang, Y. Shao, P. Mulligan, J. Qiu, L. Cao, J. Huang, *Science* **2015**, *347*, 967-970.
- [9] Y. Wu, X. Yang, W. Chen, Y. Yue, M. Cai, F. Xie, E. Bi, A. Islam, L. Han, *Nat. Energy* **2016**, *1*, 16148.
- [10] <https://www.nrel.gov/pv/assets/images/efficiency-chart.png>, The National Renewable Energy Laboratory (NREL), **2017**.
- [11] M. A. Green, K. Emery, Y. Hishikawa, W. Warta, E. D. Dunlop, *Prog. Photovoltaics: Res. Appl.* **2015**, *23*, 1-9.
- [12] X. Meng, Y. Bai, S. Xiao, T. Zhang, C. Hu, Y. Yang, X. Zheng, S. Yang, *Nano Energy* **2016**, *30*, 341-346.
- [13] M. Saliba, T. Matsui, K. Domanski, J.-Y. Seo, A. Ummadisingu, S. M. Zakeeruddin, J.-P. Correa-Baena, W. R. Tress, A. Abate, A. Hagfeldt, M. Grätzel, *Science* **2016**, *354*, 206-209.
- [14] E. J. Juarez-Perez, Z. Hawash, S. R. Raga, L. K. Ono, Y. Qi, *Energy Environ. Sci.* **2016**, *9*, 3406-3410.
- [15] K. A. Bush, C. D. Bailie, Y. Chen, A. R. Bowring, W. Wang, W. Ma, T. Leijtens, F. Moghadam, M.D. McGehee, *Adv. Mater.* **2016**, *28*, 3937-3943.
- [16] J. Huang, X. Yu, J. Xie, C.-Z. Li, Y. Zhang, D. Xu, Z. Tang, C. Cui, D. Yang, *ACS Appl. Mater. Interfaces* **2016**, *8*, 34612-34619.
- [17] A. Agresti, S. Pescetelli, L. Cinà, D. Konios, G. Kakavelakis, E. Kymakis, A D. Carlo, *Adv. Funct. Mater.* **2016**, *26*, 2686-2694.
- [18] J. Pan, C. Mu, Q. Li, W. Li, D. Ma, D. Xu, *Adv. Mater.* **2016**, *28*, 8309-8314.

- [19] X. Song, W. Wang, P. Sun, W. Ma, Z.-K. Chen, *Appl. Phys. Lett.* **2015**, *106*, 033901.
- [20] P.-W. Liang, C.-Y. Liao, C.-C. Chueh, F. Zuo, S. T. Williams, X.-K. Xin, J. Lin, A. K. Y. Jen, *Adv. Mater.* **2014**, *26*, 3748-3754.
- [21] Y. Sheng, Y. Hu, A. Mei, P. Jiang, X. Hou, M. Duan, L. Hong, Y. Guan, Y. Rong, Y. Xiong, H. Han, *J. Mater. Chem. A* **2016**, *4*, 16731-16736.
- [22] Y. Xue, Y. Wu, Y. Li, *J. Power Sources* **2017**, *344*, 160-169.
- [23] X. Zhao, F. Zhang, C. Yi, D. Bi, X. Bi, P. Wei, J. Luo, X. Liu, S. Wang, X. Li, S. M. Zakeeruddin, M. Gratzel, *J. Mater. Chem. A* **2016**, *4*, 16330-16334.
- [24] J.-W. Lee, D.-H. Kim, H.-S. Kim, S.-W. Seo, S.-M. Cho, N.-G. Park, *Adv. Energy Mater.* **2015**, *5*, 1501310.
- [25] W. Qiu, A. Ray, M. Jaysankar, T. Merckx, J. P. Bastos, D. Cheyons, R. Gehlhaar, J. Poortmans, P. Heremans, *Adv. Funct. Mater.* **2017**, *27*, 1700920.
- [26] X. Zhang, X. Ren, B. Liu, R. Munir, X. Zhu, D. Yang, J. Li, Y. Liu, D.-M. Smilgies, R. Li, Z. Yang, T. Niu, X. Wang, A. Amassian, K. Zhao, S. Liu, *Energy Environ. Sci.* **2017**, *10*, 2095-2102.
- [27] G. E. Eperon, S. D. Stranks, C. Menelaou, M. B. Johnston, L. M. Herz, H. J. Snaith, *Energy Environ. Sci.* **2014**, *7*, 982-988.
- [28] H.-S. Kim, J.-Y. Seo, N.-G. Park, *ChemSusChem* **2016**, *9*, 2528-2540.
- [29] R. G. Niemann, L. Gouda, J. Hu, S. Tirosh, R. Gottesman, P. J. Cameron, A. Zaban, *J. Mater. Chem. A* **2016**, *4*, 17819-17827.
- [30] N. J. Jeon, J. H. Noh, W. S. Yang, Y. C. Kim, S. Ryu, J. Seo, S. I. Seok, *Nature* **2015**, *517*, 476.

- [31] Y. H. Park, I. Jeong, S. Bae, H. J. Son, P. Lee, J. Lee, C.-H. Lee, M. J. Ko, *Adv. Funct. Mater.* **2017**, *27*, 1605988.
- [32] N. Zhou, Y. Shen, Y. Zhang, Z. Xu, G. Zheng, L. Li, Q. Chen, H. Zhou, *Small* **2017**, *13*, 1700484.
- [33] G. Divitini, S. Cacovich, F. Matteocci, L. Cina, A. Di Carlo, C. Ducati, *Nat. Energy* **2016**, *1*, 15012.
- [34] D. Bi, P. Gao, R. Scopelliti, E. Oveisi, J. Luo, M. Grätzel, A. Hagfeldt, M. K. Nazeeruddin, *Adv. Mater.* **2016**, *28*, 2910-2915.
- [35] X. Zhang, J. Ye, L. Zhu, H. Zheng, G. Liu, X. Liu, B. Duan, X. Pan, S. Dai, *Nanoscale* **2017**, *9*, 4691-4699.
- [36] Q. Shen, Y. Ogomi, J. Chang, T. Toyoda, K. Fujiwara, K. Yoshino, K. Sato, K. Yamazaki, M. Akimoto, Y. Kuga, K. Katayama, S. Hayase, *J. Mater. Chem. A* **2015**, *3*, 9308-9316.
- [37] Y. Ogomi, K. Kukihara, S. Qing, T. Toyoda, K. Yoshino, S. Pandey, H. Momose, S. Hayase, *ChemPhysChem* **2014**, *15*, 1062-1069.
- [38] B. Slimi, M. Mollar, I. B. Assaker, A. Kriaa, R. Chtourou, B. Mariá, *Monatshefte für Chemie-Chemical Monthly* **2017**, *148*, 835.
- [39] A. S. Subbiah, S. Agarwal, N. Mahuli, P. Nair, M. v. Hest, S, K. Sarkar, *Adv. Mater. Interfaces* **2017**, *4*, 1601143.
- [40] C. Yi, J. Luo, S. Meloni, A. Boziki, N. Ashari-Astani, C. Grätzel, S. M. Zakeeruddin, U. Rothlisberger, M. Grätzel, *Energy Environ. Sci.* **2016**, *9*, 656-662.

## Entry for the Table of Contents

Films and solar cells based on  $(\text{FAPbI}_3)_{0.9}(\text{FAPbBr}_3)_{0.1}$  by introducing different contents of MA, Cs or Rb cations are respectively prepared and systematically studied. The results demonstrate that the  $(\text{FAPbI}_3)_{0.9}(\text{FAPbBr}_3)_{0.1}$  devices with 10% Cs display a highest PCE up to 19.94% and excellent humidity and heat stability.

